Dynamical dimer method for the determination of transition states with *ab initio* molecular dynamics

Alexander Poddey[a] and Peter E. Blöchl[b]
Institute of Theoretical Physics, Clausthal University of Technology, Leibnizstrasse 10, D-38678 Clausthal-Zellerfeld, Germany

(Received 9 October 2007; accepted 27 November 2007; published online 29 January 2008)

A dynamical formulation of the dimer method for the determination of transition states is presented. The method is suited for *ab initio* molecular dynamics using the fictitious Lagrangian formulation. The method has been applied to the conrotatory ring opening of chlorocyclobutadiene, an example, where the application of the drag method is problematic. © *2008 American Institute of Physics*. [DOI: 10.1063/1.2826338]

I. INTRODUCTION

The concept of the transition state has a fundamental role for the prediction of rate constants of materials processes. The transition state is the lowest point on the energy barrier separating two metastable states representing the initial and final states of a process. The energy difference between the initial state and the transition state is the activation energy. The curvatures of the potential energy surface at the initial state and the transition state provide an estimate of entropic effects.[1,2] A molecular dynamics simulation starting from the transition state allows one to construct the dynamical trajectory of a reaction in the low-temperature limit. The extension of this latter approach to finite temperatures is straightforward.[3]

The determination of transition states is, however, substantially more difficult than the determination of minima of the total energy surface. A large number of methods have been invented and refined over the last decades (see, e.g., the Refs. 4–15 and the review articles[16,17]).

Many of these methods require the determination of the second derivatives of the total energy surface. While forces, that is, first derivatives of the potential energy surface, are readily accessible from density functional calculations, second derivatives are not, at least not without substantial effort.

An overview of methods which allow to determine transition states solely from force information can be found in Ref. 16. The most simple approach is the drag method, where a one-dimensional constraint forces the system across a reaction barrier. Widely used are also "chain of states" algorithms such as the nudged elastic band[10–12] or the string method.[14,15]

Intermediate between these extremes is the dimer method.[18] It couples two instances of the system, which we will call monomers. The monomers have a specified distance in configuration space. If the system follows the forces, after inverting of the force parallel to the dimer, it evolves to a saddle point of first order, that is, the transition state.

The original dimer method[18] applied a two step algorithm. In a first step, the potential energy of the dimer-construct is minimized, excluding parallel motion, following a conjugate gradient approach. Then a large step is taken in the direction parallel to the dimer axis. Recently, an improvement has been suggested which minimizes the number of gradient evaluations.[19]

In the context of fictitious Lagrangian approach to first-principles molecular dynamics,[20] such a two step procedure is not feasible, because the electronic wave functions must be able to follow the atomic motion adiabatically. The fictitious Lagrangian approach requires a larger number of time steps. However, the computational cost per time step is minimal. While a first-principles string approach has been published recently,[21] the dimer method has not been examined in the framework of *ab initio* molecular dynamics.

In the present study, we introduce a dynamical formulation of the dimer method. Starting from an extended Lagrangian for the dimer in the configuration space with doubled dimensionality, we derive equations of motion that, in the presence of dissipation, converge at transition states of first order. An analysis of the trajectories of the dimer close to the stable points provides information on the stability and gives guidance for improving the performance of the method. The method has been implemented in the CP-PAW code and has been applied to the conrotatory ring opening of chlorocyclobutene, an example where the conventional drag method fails unless special precautions are taken.

The paper is organized as follows. In Sec. II we define the extended Lagrangian for the dimer motion and derive the equations of motion. In Sec. III we analyze stability and the dynamics in the proximity of the stable points. Section IV is devoted to the discretization the equations of motion and the aspects of the actual implementation. In Sec. V, the method is applied to the conrotatory ring opening of cyclobutene as practical example and compared to the drag method.

II. LAGRANGIAN AND EQUATIONS OF MOTION

In this section we define the Lagrangian underlying the present work and derive the equations of motion. We begin by defining our notation and we introduce a convenient set of coordinates.

[a]Electronic mail: alexander.poddey@tu-clausthal.de.
[b]Electronic mail: peter.bloechl@tu-clausthal.de.

The dimer consists of two points in configurational space separated by a fixed distance. We use mass-weighted coordinates $\mathbf{x}_i$ defined as

$$\mathbf{x}_i := \mathbf{m}^{1/2}\mathbf{R}_i, \tag{1}$$

where the vectors $\mathbf{R}_i$ with $i=1,2$ are the positions of the two monomers forming the dimer in configurational space. For a system with N atoms each vector has $3N$ dimensions. In addition, each monomer has its own set of electronic wave functions. The mass matrix $\boldsymbol{m}$ is diagonal and the masses of the respective atoms are located on the main diagonal.

It is convenient to introduce a variable transformation into center-of-gravity coordinates $\mathbf{Y}_1$ and relative coordinates $\mathbf{Y}_2$,

$$\mathbf{Y}_1 = \frac{\mathbf{x}_1 + \mathbf{x}_2}{2}, \tag{2}$$

$$\mathbf{Y}_2 = \mathbf{x}_1 - \mathbf{x}_2. \tag{3}$$

Loosely speaking $\mathbf{Y}_1$ describes the mean structure of the molecule, while $\mathbf{Y}_2$ describes the orientation of the dimer.

A dimer has three basic types of motion: motion parallel to the dimer axis ($\mathbf{v}_\parallel$), motion perpendicular to the axis ($\mathbf{v}_\perp$), and rotation about the center of gravity ($\mathbf{v}_\circ$). In the following, we divide the velocities into the contributions from these basic types of motion. The corresponding velocities are

$$\mathbf{v}_\circ = \dot{\mathbf{Y}}_2 = \dot{\mathbf{x}}_1 - \dot{\mathbf{x}}_2, \tag{4}$$

$$\mathbf{v}_\parallel = \frac{\mathbf{Y}_2 \otimes \mathbf{Y}_2}{d^2}\dot{\mathbf{Y}}_1 = (\mathbf{x}_1 - \mathbf{x}_2)\frac{(\mathbf{x}_1 - \mathbf{x}_2)(\dot{\mathbf{x}}_1 + \dot{\mathbf{x}}_2)}{2d^2}, \tag{5}$$

$$\mathbf{v}_\perp = \left(1 - \frac{\mathbf{Y}_2 \otimes \mathbf{Y}_2}{d^2}\right)\dot{\mathbf{Y}}_1 = \frac{\dot{\mathbf{x}}_1 + \dot{\mathbf{x}}_2}{2} - \mathbf{v}_\parallel. \tag{6}$$

The dot denotes the time derivative, and d is the so called "dimer distance" $d=\sqrt{\mathbf{Y}_2^2}=\sqrt{(\mathbf{x}_1-\mathbf{x}_2)^2}$. The symbol $\otimes$ refers to the outer product defined by $(\mathbf{a}\otimes\mathbf{b})\mathbf{c}=\mathbf{a}(\mathbf{b}\cdot\mathbf{c})$. Note, that $\mathbf{Y}_2\otimes\mathbf{Y}_2/d^2$ is an operator that projects a vector onto the dimer axis.

Now we define our theory by setting up a Lagrangian function in the relative and center-of-gravity coordinates,

$$\begin{aligned}\mathcal{L}(\mathbf{Y}_1,\mathbf{Y}_2,\dot{\mathbf{Y}}_1,\dot{\mathbf{Y}}_2) = {} & M_\circ \tfrac{1}{4}\mathbf{v}_\circ^2 + M_\perp \mathbf{v}_\perp^2 + M_\parallel \mathbf{v}_\parallel^2 \\ & - V\left(\mathbf{m}^{-1/2}\left[\mathbf{Y}_1 + \tfrac{1}{2}\mathbf{Y}_2\right]\right) \\ & - V\left(\mathbf{m}^{-1/2}\left[\mathbf{Y}_1 - \tfrac{1}{2}\mathbf{Y}_2\right]\right) \\ & - \bar{\lambda}[\mathbf{Y}_2^2 - d^2].\end{aligned} \tag{7}$$

The potential energy is described by the potential energy surface $V(\mathbf{R})$. The velocities $\mathbf{v}_\circ$, $\mathbf{v}_\perp$, and $\mathbf{v}_\parallel$ are to be treated as functions of $\mathbf{Y}_1$ and $\mathbf{Y}_2$ and their time derivatives $\dot{\mathbf{Y}}_1$ and $\dot{\mathbf{Y}}_2$ as defined in Eqs. (4)–(6).

We introduced three scale factors ($M_\circ$, $M_\parallel$, and $M_\perp$) that allow us to scale the masses for the three types of motions independently, which will later be used to accelerate convergence. More importantly, by choosing a negative value of $M_\parallel$, the motion along the dimer direction is inverted, so that the dimer climbs up the barrier.

If the scale factors are equal to one, the conventional kinetic energy is recovered, that is,

$$\tfrac{1}{4}\mathbf{v}_\circ^2 + \mathbf{v}_\parallel^2 + \mathbf{v}_\perp^2 = \tfrac{1}{2}\dot{\mathbf{R}}_1\mathbf{m}\dot{\mathbf{R}}_1 + \tfrac{1}{2}\dot{\mathbf{R}}_2\mathbf{m}\dot{\mathbf{R}}_2. \tag{8}$$

Using the method of Lagrange multipliers, a term has been introduced to describe the dimer-distance constraint,

$$\mathbf{Y}_2^2 = d^2, \tag{9}$$

which ensures that the dimer distance in mass-weighted coordinates is equal to d. The corresponding Lagrange multiplier is denoted by $\bar{\lambda}$.

In addition to the Lagrangian we also define a Rayleigh's dissipation function $\mathcal{D}$,

$$\mathcal{D} = \gamma_\circ M_\circ \tfrac{1}{4}\mathbf{v}_\circ^2 + \gamma_\parallel M_\parallel \mathbf{v}_\parallel^2 + \gamma_\perp M_\perp \mathbf{v}_\perp^2, \tag{10}$$

which allows us to introduce dissipation in a consistent manner.

The Euler-Lagrange equation for the Lagrangian of Eq. (7) and the Rayleigh's dissipation function from Eq. (10) are obtained from

$$\frac{d}{dt}\frac{\partial \mathcal{L}}{\partial \dot{Y}_{i,n}} - \frac{\partial \mathcal{L}}{\partial Y_{i,n}} + \frac{\partial \mathcal{D}}{\partial \dot{Y}_{i,n}} = 0, \tag{11}$$

where the index $i\in\{1,2\}$ labels the two monomers, and $n\in\{1,\ldots,3N\}$ labels the coordinate in configuration space.

The resulting equations of motion have the following forms:

$$\begin{aligned}&\left(1 - \frac{\mathbf{Y}_2 \otimes \mathbf{Y}_2}{d^2}\right)M_\perp(\ddot{\mathbf{Y}}_1 + \gamma_\perp \dot{\mathbf{Y}}_1) \\ &\quad + \left(\frac{\mathbf{Y}_2 \otimes \mathbf{Y}_2}{d^2}\right)M_\parallel(\ddot{\mathbf{Y}}_1 + \gamma_\parallel \dot{\mathbf{Y}}_1) - \frac{1}{2}\mathbf{m}^{-1/2}(\mathbf{F}_1 + \mathbf{F}_2) \\ &\quad + (M_\parallel - M_\perp)\left[\frac{d}{dt}\left(\frac{\mathbf{Y}_2 \otimes \mathbf{Y}_2}{d^2}\right)\right]\dot{\mathbf{Y}}_1 = 0\end{aligned} \tag{12}$$

and

$$\begin{aligned}&M_\circ \ddot{\mathbf{Y}}_2 - m^{-1/2}(\mathbf{F}_1 - \mathbf{F}_2) + 4\lambda \mathbf{Y}_2 + 4(M_\perp - M_\parallel)\frac{\mathbf{Y}_2\dot{\mathbf{Y}}_1}{d^2}\dot{\mathbf{Y}}_1 \\ &\quad + \gamma_\circ M_\circ \dot{\mathbf{Y}}_2 = 0.\end{aligned} \tag{13}$$

Here we have used the forces acting on the monomers defined as

$$\mathbf{F}_i := -\left.\nabla\right|_{\mathbf{R}_i} V. \tag{14}$$

In Eq. (13) we absorbed all terms which lead to a force parallel to the dimer axis into the constraint force by redefining the Lagrange multiplier. Thus the variable λ used in Eq. (13) differs from the Lagrange multiplier $\bar{\lambda}$ in Eq. (7).

Furthermore, because the dimer system moves on the hyperplane with constant dimer distance, we simplified the final equations by using

$$\mathbf{Y}_2^2 = d^2 \tag{15}$$

and

$$\frac{\partial}{\partial t}\mathbf{Y}_2^2 = 0. \tag{16}$$

Equation (12) describes the motion of the center of gravity of the dimer, which is related to the structure of the molecule. Equation (13) describes the orientational motion of the dimer.

III. LOCAL STABILITY ANALYSIS

For $M_\circ = M_\parallel = M_\perp = 1$, the Lagrange function [Eq. (7)] describes a physical system of two mass points moving in a potential V under the influence of the constraint force that keeps the dimer distance invariant. With positive friction factors, $\gamma_\circ$, $\gamma_\parallel$, and $\gamma_\perp$, the dimer will come to rest with the center-of-gravity coordinate next to a local minimum. The dimer axis will be aligned nearly parallel to the lowest vibrational eigenmode. The above statements are exactly fulfilled in the limit of vanishing dimer distance.

If we choose a negative value of $M_\parallel$, the motion will become unstable near local minima. Instead, the dimer will be attracted by transition states of first order. A transition state of first order is characterized by the presence of exactly one eigenmode with an imaginary frequency.

These properties of the dynamics have been derived from the following local stability analysis. First we determine the stationary points for the dimer dynamics. Then we investigate the dynamics in the neighborhood of those stationary points.

For this analysis we can replace the potential energy surface by its truncated Taylor expansion at a given point $\mathbf{R}^{(0)} = \mathbf{m}^{-1/2}\mathbf{x}^{(0)}$, namely,

$$V(\mathbf{R}) = V^{(0)} - \mathbf{F}^{(0)}\mathbf{R} + \tfrac{1}{2}(\mathbf{R} - \mathbf{R}^{(0)})\mathbf{m}^{1/2}\mathbf{D}\mathbf{m}^{1/2}(\mathbf{R} - \mathbf{R}^{(0)}), \tag{17}$$

with the dynamical matrix $\mathbf{D}$ defined as

$$D_{i,j} = \frac{1}{\sqrt{m_{i,i}}} \left.\frac{\partial^2 V}{\partial R_i \partial R_j}\right|_{\mathbf{R}^{(0)}} \frac{1}{\sqrt{m_{j,j}}}. \tag{18}$$

From Eqs. (17) and (1), we obtain the forces

$$\mathbf{F}(\mathbf{x}) = \mathbf{F}^{(0)} - \mathbf{m}^{1/2}\mathbf{D}(\mathbf{x} - \mathbf{x}^{(0)}). \tag{19}$$

A. Stationary points

If we insert the condition for a stationary point defined by $\dot{\mathbf{Y}}_i = \ddot{\mathbf{Y}}_i = 0$ in the equation of motion [Eq. (12)], we find that the forces for the two monomers at the stationary point are antiparallel and of the same magnitude. Using the Taylor expansion Eq. (19) in the equation of motion [Eq. (12)], we find that the center of gravity of the dimer $\mathbf{Y}_1$ lies at a stationary point of the potential, if the dimer is stationary, that is,

$$\mathbf{F}(\mathbf{Y}_1) = 0. \tag{20}$$

Similarly from Eqs. (13) and (19) we obtain

$$\mathbf{D}\mathbf{Y}_2 = -4\lambda\mathbf{Y}_2. \tag{21}$$

Thus the dimer axis points along an eigenvector of the dynamical matrix.

In conclusion, we find that the dimer dynamics is stationary, when its center of gravity lies at an extremum or a saddle point of the potential energy surface and when, in addition, the dimer axis points along one of the vibrational eigenmodes.

B. Linearized equation of motion

Without loss of generality, we choose in the following a coordinate system for which the stationary point of the potential energy surface lies at the origin. Secondly, we denote the eigenvectors of the dynamical matrix as $\mathbf{e}_i$, with $\mathbf{e}_i\mathbf{e}_j = \delta_{i,j}$, and the corresponding eigenvalues with ω_i^2. The eigenvector, which is parallel to the dimer axis, is denoted by $\bar{\mathbf{e}}$ and the corresponding eigenvalue is denoted by $\bar{\omega}^2$. Thus, with Eq. (21), we can identify the Lagrange multiplier as $\lambda = -\frac{1}{4}\bar{\omega}^2$.

Linearization of the equations of motion [Eqs. (12) and (13)] about $\mathbf{Y}_1 = 0$ and $\mathbf{Y}_2 = \bar{\mathbf{e}}d$ with $\mathbf{F}^{(0)} = 0$ yields the following equations for the deviations $\delta\mathbf{Y}_1(t)$ and $\delta\mathbf{Y}_2(t)$ from the stationary point:

$$(1 - \bar{\mathbf{e}} \otimes \bar{\mathbf{e}})M_\perp(\delta\ddot{\mathbf{Y}}_1 + \gamma_\perp\delta\dot{\mathbf{Y}}_1) + (\bar{\mathbf{e}} \otimes \bar{\mathbf{e}})M_\parallel(\delta\ddot{\mathbf{Y}}_1 + \gamma_\parallel\delta\dot{\mathbf{Y}}_1) + \mathbf{D}\delta\mathbf{Y}_1 = 0, \tag{22}$$

$$M_\circ\delta\ddot{\mathbf{Y}}_2 + \mathbf{D}\delta\mathbf{Y}_2 + \bar{\omega}^2\delta\mathbf{Y}_2 + M_\circ\gamma_\circ\delta\dot{Y}_2 = 0. \tag{23}$$

We project the second equation [Eq. (23)] onto the eigenvectors $\mathbf{e}_i$ and obtain

$$M_\circ(\mathbf{e}_i\delta\ddot{\mathbf{Y}}_2) + (\omega_i^2 - \bar{\omega}^2)(\mathbf{e}_i\delta\mathbf{Y}_2) + M_\circ\gamma_\circ(\mathbf{e}_i\delta\dot{Y}_2) = 0. \tag{24}$$

Note that the motion along $\bar{\mathbf{e}}$ is simple due to the distance constraint. The frequency of the variable $\mathbf{e}_i\mathbf{Y}_2$ is therefore

$$\omega_\circ = \pm\sqrt{\frac{\omega_i^2 - \bar{\omega}^2}{M_\circ}}. \tag{25}$$

We see that, for a positive mass $M_\circ$, the dynamics is stable only if $\bar{\omega}^2$ is the lowest eigenvalue of the dynamical matrix. Thus the dimer axis will always orient along the eigenvector with the lowest eigenvalue.

Now, we project Eq. (22) onto the eigenvector $\bar{\mathbf{e}}$ of the dynamical matrix,

$$M_\parallel(\bar{\mathbf{e}}\delta\ddot{\mathbf{Y}}_1) + \bar{\omega}^2(\bar{\mathbf{e}}\delta\mathbf{Y}_1) + M_\parallel\gamma_\parallel(\bar{\mathbf{e}}\delta\dot{\mathbf{Y}}_1) = 0, \tag{26}$$

which yields the translational motion of the dimer along the dimer axis. This equation will be responsible for the ascent to a saddle point. The eigenfrequency of the variable $\bar{\mathbf{e}}\mathbf{Y}_1$ is

$$\omega_\parallel = \pm\frac{\bar{\omega}}{\sqrt{M_\parallel}}. \tag{27}$$

For a negative mass $M_\parallel$, which is the choice for a transition state search, Eq. (26) is stable only if the dimer is oriented along an unstable vibrational mode of the potential energy

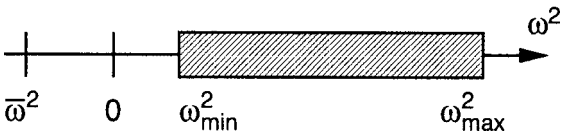

FIG. 1. Sketch of the eigenvalue spectrum of the dynamical matrix at the saddle point of first order with the definition of $\omega_{\min}$ and $\omega_{\max}$.

surface, that is, with the dimer oriented along an eigenvector $\bar{\mathbf{e}}$ with an imaginary frequency.

Now, we project Eq. (22) onto the eigenvectors $\mathbf{e}_i$ with $\mathbf{e}_i \perp \bar{\mathbf{e}}$ and we obtain

$$M_\perp(\mathbf{e}_i \delta\ddot{\mathbf{Y}}_1) + \omega_i^2(\mathbf{e}_i \delta\mathbf{Y}_1) + M_\perp \gamma_\perp(\mathbf{e}_i \delta\dot{\mathbf{Y}}_1) = 0, \tag{28}$$

which represents the translational motion perpendicular to the dimer axis. The translational motion is related to an optimization of the atomic structure. The frequency of the variable $\mathbf{e}_i\mathbf{Y}_1$ with $\mathbf{e}_i \perp \bar{\mathbf{e}}$ is

$$\omega_\perp = \frac{\omega_i}{\sqrt{M_\perp}}. \tag{29}$$

From Eqs. (25), (27), and (29) we find that the dimer with positive $M_\circ$ and $M_\perp$ and negative $M_\parallel$ will only come to rest at transition states of first order, that is, if $\bar{\omega}^2 < 0$ and if all other eigenvalues are positive. In that case the dimer axis points along the eigenvector corresponding to the imaginary frequency, that is, across the saddle point.

C. Masses and frictions

We will later solve the equations of motion [Eqs. (12) and (13)] with the Verlet algorithm. The Verlet algorithm for a harmonic oscillator with a frequency ω becomes unstable if the time step Δ used for the discretization of the equation of motion is smaller than $2/\omega$. The frequency of the discretized motion is accurate to within 1% if $\omega\Delta < \pi/5$. Thus, it is important to understand the vibrational spectrum, shown schematically in Fig. 1, of the motion in the potential.

Thus, the stability limit requires us to choose the masses as

$$M_\parallel < \frac{\bar{\omega}^2\Delta^2}{8}, \tag{30}$$

$$M_\perp > \frac{\omega_{\max}^2\Delta^2}{8}, \tag{31}$$

$$M_\circ > \frac{(\omega_{\max}^2 - \omega_{\min}^2)\Delta^2}{4}. \tag{32}$$

In order to minimize the number of time steps, it is desirable to choose the masses close to these limits.

Let us now obtain an *a priori* estimate of these limits: (1) For practical purposes, we can make the assumption that $\omega_{\min} \ll \omega_{\max}$ and thus we set $\omega_{\min}$ to zero. (2) The highest vibrational mode is that of H_2, with a frequency of 4400 cm^{-1}. Frequencies for bond-stretch vibrations are of the order 1000 cm^{-1}. These numbers are reasonable upper estimates for $\omega_{\max}$. (3) The absolute value of the imaginary frequency at the saddle point is typically in the range of the high-lying real-frequency modes that is comparable to $\omega_{\max}$. Hence $\bar{\omega}^2 \approx -\omega_{\max}^2$. With these assumptions we obtain the following recommended values for the masses:

$$M_\parallel = -\kappa\Delta^2, \tag{33}$$

$$M_\perp = \kappa\Delta^2, \tag{34}$$

$$M_\circ = 2\kappa\Delta^2, \tag{35}$$

where $\kappa = (6 \times 10^{-3}\ \text{a.u.})^2$ is a recommended constant based on the H_2 vibration.

Let us now turn our attention to the friction values. The goal is to reach an optimum convergence at the stationary point of the dimer. For a damped harmonic oscillator,

$$m\ddot{x} = -m\omega_0^2 x - m\gamma x, \tag{36}$$

the fastest decay rate as a function of the friction is obtained for critical damping, that is, in between the oscillatory and the overdamped regime. Critical damping is obtained for a friction of $\gamma = 2\omega_0$. Thus we choose

$$\gamma_\parallel = 2\sqrt{\frac{\bar{\omega}^2}{M_\parallel}}, \tag{37}$$

$$2\sqrt{\frac{\omega_{\min}^2}{M_\perp}} < \gamma_\perp < 2\sqrt{\frac{\omega_{\max}^2}{M_\perp}}, \tag{38}$$

$$2\sqrt{\frac{\omega_{\min}^2 - \bar{\omega}^2}{M_\circ}} < \gamma_0 < 2\sqrt{\frac{\omega_{\max}^2 - \bar{\omega}^2}{M_\circ}}. \tag{39}$$

Note that a too high friction freezes out those modes in the overdamped regime. Thus it is usually better to use a friction near the lower bound of the sensible regime.

IV. NUMERICAL INTEGRATION OF THE EQUATIONS OF MOTION

A. Discretization of the equations of motion

The equations of motion [Eqs. (12) and (13)] are nonlinear in the velocities. This leads to a nonlinear equation for the discretized equation of motion. We tackle the problem by iterating on the nonlinear terms in the velocities.

We set up the discretized equations of motion while treating the terms nonlinear in the velocities as an abstract force,

$$\mathbf{G}_1 := -(M_\parallel - M_\perp)\left[\frac{d}{dt}\left(\frac{\mathbf{Y}_2 \otimes \mathbf{Y}_2}{d^2}\right)\right]\dot{\mathbf{Y}}_1, \tag{40}$$

$$\mathbf{G}_2 := 4(M_\parallel - M_\perp)\frac{\mathbf{Y}_2\dot{\mathbf{Y}}_1}{d^2}\dot{\mathbf{Y}}_1. \tag{41}$$

The equations of motion are discretized according to the Verlet algorithm,

$$\dot{y} \to \frac{y(+) - y(-)}{2\Delta}, \tag{42}$$

$$\ddot{y} \to \frac{y(+) - 2y(0) + y(-)}{\Delta^2}, \tag{43}$$

where Δ is the discretization time step, and where we used the short-hand notation

$$y(+) = y(t + \Delta), \tag{44}$$

$$dy(0) = y(t), \tag{45}$$

$$y(-) = y(t - \Delta). \tag{46}$$

From Eq. (12) we obtain

$$\left(1 - \frac{\mathbf{Y}_2 \otimes \mathbf{Y}_2}{d^2}\right)\frac{M_\perp}{\Delta^2}\{(1 + a_\perp)\mathbf{Y}_1(+) - 2\mathbf{Y}_1(0) + (1 - a_\perp)\mathbf{Y}_1(-)\} + \left(\frac{\mathbf{Y}_2 \otimes \mathbf{Y}_2}{d^2}\right)\frac{M_\parallel}{\Delta^2}\{(1 + a_\parallel)\mathbf{Y}_1(+) - 2\mathbf{Y}_1(0) + (1 - a_\parallel)\mathbf{Y}_1(-)\} - \frac{1}{2}\mathbf{m}^{-1/2}(\mathbf{F}_1 + \mathbf{F}_2) - \mathbf{G}_1 = 0, \tag{47}$$

where $a_\perp = \gamma_\perp \Delta/2$ and $a_\parallel = \gamma_\parallel \Delta/2$. In the projectors we have dropped the argument of $\mathbf{Y}_2(0)$.

Equation (47) can be resolved for $\mathbf{Y}_1(+)$ by multiplication with

$$\left(1 - \frac{\mathbf{Y}_2 \otimes \mathbf{Y}_2}{d^2}\right)\frac{\Delta^2}{M_\perp(1 + a_\perp)} + \left(\frac{\mathbf{Y}_2 \otimes \mathbf{Y}_2}{d^2}\right)\frac{\Delta^2}{M_\parallel(1 + a_\parallel)}. \tag{48}$$

The result is

$$\mathbf{Y}_1(+) = \left(1 - \frac{\mathbf{Y}_2 \otimes \mathbf{Y}_2}{d^2}\right)\left\{\frac{2}{1 + a_\perp}\mathbf{Y}_1(0) - \frac{1 - a_\perp}{1 + a_\perp}\mathbf{Y}_1(-) + \left(\frac{1}{2}\mathbf{m}^{-1/2}(\mathbf{F}_1 + \mathbf{F}_2) + \mathbf{G}_1\right)\frac{\Delta^2}{M_\perp(1 + a_\perp)}\right\} + \left(\frac{\mathbf{Y}_2 \otimes \mathbf{Y}_2}{d^2}\right)\left\{\frac{2}{1 + a_\parallel}\mathbf{Y}_1(0) - \frac{1 - a_\parallel}{1 + a_\parallel}\mathbf{Y}_1(-) + \left(\frac{1}{2}\mathbf{m}^{-1/2}(\mathbf{F}_1 + \mathbf{F}_2) + \mathbf{G}_1\right)\frac{\Delta^2}{M_\parallel(1 + a_\parallel)}\right\}. \tag{49}$$

Similarly we discretize the equation of motion for the dimer distance [Eq. (13)]. Following Ryckaert *et al.*,[22] we first propagate without the force of constraint to obtain

$$\bar{\mathbf{Y}}_2 = \frac{2}{1 + a_\circ}\mathbf{Y}_2(0) - \frac{1 - a_\circ}{1 + a_\circ}\mathbf{Y}_2(-) + (\mathbf{m}^{-1/2}(\mathbf{F}_1 - \mathbf{F}_2) + \mathbf{G}_2)\frac{\Delta^2}{M_\circ(1 + a_\circ)}, \tag{50}$$

with $a_\circ = \gamma_\circ \Delta/2$. The new vector $\mathbf{Y}_2(+)$ is related to $\bar{Y}_2$ by the constraint force and the Lagrange parameter λ according to

$$\mathbf{Y}_2(+) = \bar{\mathbf{Y}}_2 - 4\lambda\mathbf{Y}_2(0)\frac{\Delta^2}{M_\circ(1 + a_\circ)}. \tag{51}$$

The Lagrange parameter is then adjusted so that the constraint $Y_2^2(+) = d^2$, namely, a given dimer length, is satisfied.

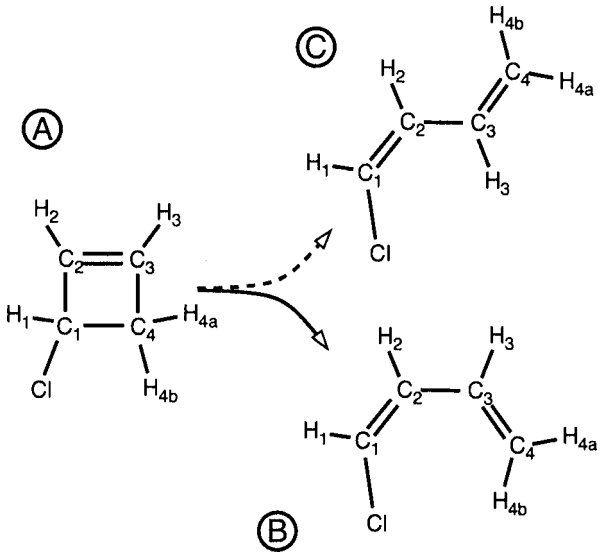

FIG. 2. Initial state, 1-chloro-2-cyclobutene (A), and final state, 1-chloro-buta-1,3-diene (B), for the conrotatory ring opening of chlorocyclobutene. Also shown is the product of the disrotatory ring opening, trans-1-chloro-buta-1,3-diene (C).

In the first iteration we estimate this forces $\mathbf{G}_1$ and $\mathbf{G}_2$ from the previous iterations or we set them to zero. Then we propagate the positions, which provides us with a better estimate for the nonlinear terms. This loop is then iterated to convergence.

B. Restricting the orientation of the dimer

It will be important to limit the degrees of freedom, in which the two monomers may differ. This implies restricting the orientation of the dimer to a space with lower-dimensionality. The reason is to prevent the dimers from converging at irrelevant saddle points, which are not of interest. This is a common problem for complex systems that exhibit many minima and saddle points. This restriction is accomplished easily by setting the corresponding components of $\mathbf{Y}_2$ in Eq. (50) to zero.

V. APPLICATION: CONROTATORY RING OPENING OF 1-CHLORO-2-CYCLOBUTENE

In order to demonstrate the performance of the dimer method described above, we have chosen a prototypical system for tests of transition state searches, namely, the ring opening of cyclobutene. The isomerization of cyclobutene to *cis*-butadiene is the prototypical example of concerted stereospecific reactions. The underlying processes have been studied and discussed extensively by several groups[23–26] (and references therein). The potential energy surfaces of the con- as well as of the disrotatory isomerization mechanisms exhibit principal structures, which render the determination of the corresponding transition states complicated.[24]

In order to avoid special effects due to the high symmetry of cyclobutene, that would be untypical for other molecules, we explored 1-chloro-2-cyclobutene. This molecule and the two relevant reaction products are shown in Fig. 2.

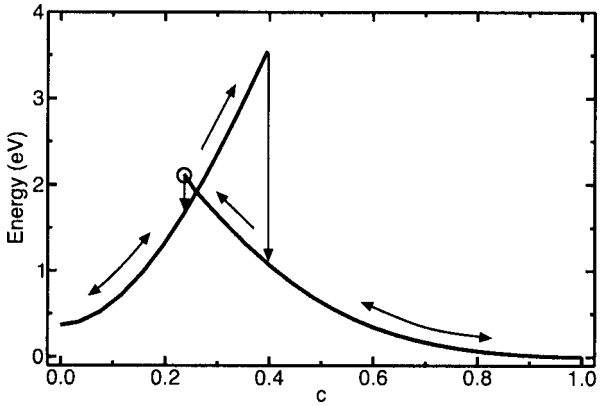

FIG. 3. Potential energy relative to the energy of final state (B) over reaction coordinate from a forward and backward calculation using the drag method. The true transition state (determined using the dynamical dimer method) is denoted by a circle.

Computational details of our calculations are given in Appendix A. The coordinates of the structures are supplied with the supplementary material.[27]

A. Drag calculations

In this section we investigate the reaction using the drag method. Because of its simplicity, the drag method is widely used for transition state search. However, the drag method fails for a number of systems. In such cases the energy exhibits a hysteresis effect, that is, different energy profiles are obtained when dragging the reaction coordinate in the opposite directions. The ring opening of cyclobutene is one example where the drag method exhibits a hysteresis effect.

In the drag method one specifies a one-dimensional reaction coordinate. Then one maps the energy profile along the reaction coordinate and determines the highest point as the transition state. Each point along the energy profile corresponds to the local energy minimum on a hyperplane perpendicular to the reaction coordinate. In our case we selected the reaction coordinate by the difference between initial and final states. A hyperplane with a specified value c of the reaction coordinate is given by

$$\frac{(\mathbf{R}_B - \mathbf{R}_A)(\mathbf{R} - \mathbf{R}_A)}{(\mathbf{R}_B - \mathbf{R}_A)^2} = c. \tag{52}$$

Hence the value of the reaction coordinate is zero for the initial state (A) and one for the final state (B).

In addition to the reaction coordinate, we imposed six additional constraints to avoid translations and rotations of the molecule. We have chosen

$$\tfrac{1}{2}(\mathbf{R}(C_2) + \mathbf{R}(C_3)) = 0, \tag{53}$$

$$z(C_1) = z(C_4) = \tfrac{1}{2}(x(C_1) + x(C_4)) = 0, \tag{54}$$

where the coordinates correspond to the atoms given in the parenthesis. The notation follows Fig. 2.

When the energy profile is determined by varying the reaction coordinate in small steps, once from zero to one and then from one to zero, we obtain the hysteresis shown in Fig. 3. The highest point of the energy profile is not the transition state. Instead, the highest point of each branch is an upper bound for the activation energy, while the crossing of the two branches is a lower bound.

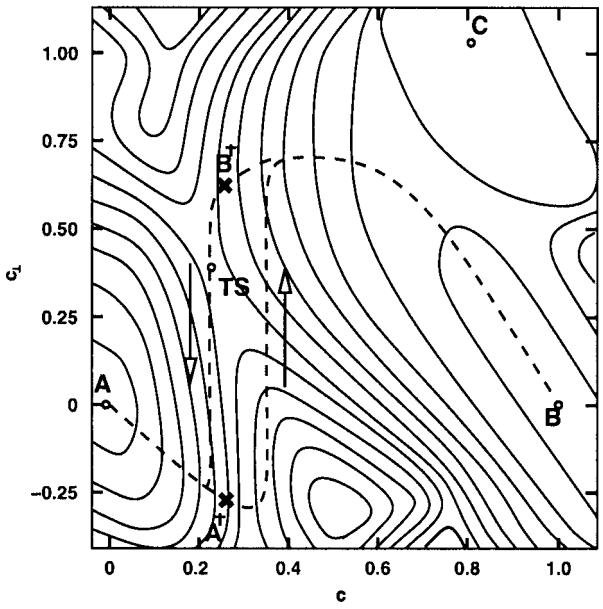

FIG. 4. Sketch of the potential energy surface of the conrotatory isomerization of 1-chloro-2-cyclobutene to 1-chloro-buta-1,3-diene. The dashed lines trace the paths obtained from drag calculations for the transitions A→B and B→A, respectively. The crosses denote the structures $A^\dagger$ and $B^\dagger$. TS corresponds to the transition state.

In order to show the underlying reason for the hysteresis, we show in Fig. 4 the total energy surface in a two-dimensional hypersurface. The two axes are the reaction coordinate and the coordinate defined by the two isoenergetic structures at the crossing of the two branches of the energy profile in Fig. 3. For each point in the two-dimensional plot the energy is at a local minimum of the $(3N-2)$-dimensional hypersurface.

We see that the drag method in the forward direction leads into a side valley that leads further onto a ridge. The point where this path becomes unstable, and from where it leads down into the valley of the product state, lies past the transition state. In the backward direction a similar instability occurs, even though closer to the reaction coordinate of the transition state.

Note that the two configurations $A^\dagger$ and $B^\dagger$, which mark the crossing of the two branches in the energy profile shown in Fig. 3, lie far from the transition state. For further information see Table I.

B. Dynamical dimer calculations

In this section we describe technical issues for dynamical dimer calculations and demonstrate their performance.

We use the fictitious Lagrangian formulation of *ab initio* molecular dynamics. This implies that the wave function coefficients and nuclei obey Newton's equation of motion, to which we added a friction, which allows to quench the system.

Special attention should be given to the wave function dynamics. The wave function cloud tied to the atoms results

TABLE I. Predicted transition state energy [relative to final state (B)] and deviation from the exact transition state for the conrotatory isomerization of 1-chloro-2-cyclobutene to 1-chloro-buta-1,3-diene. The results include three different dynamical dimer optimization strategies [(1), (2), and (3)] described in the text and the forward as well as the backward drag calculation shown in Fig. 3.

	Predicted energy (eV)	$\lvert\mathbf{R}^{\mathrm{TS}}-\mathbf{R}\rvert$ (Å)
Transition state[a]	2.110	···
	(1)	
1000 steps	2.110	1.00
1500 steps	2.111	0.85
2000 steps	2.111	0.71
	(2)	
1000 steps	2.258	0.62
1500 steps	2.116	0.37
2000 steps	2.110	0.36
	(3)	
1000 steps	2.133	1.58
1500 steps	2.112	0.85
2000 steps	2.110	0.85
TS $A \rightarrow B$	3.461	2.57
TS $B \rightarrow A$	2.120	0.56

[a]Determined by the use of a well converged dynamical dimer calculation with a final dimer distance of 0.125 Å.

in an increased effective mass of the nuclei. Furthermore, a friction applied to the wave function dynamics acts like an effective friction on the nuclear motion. For a normal ground-state search, this is not problematic. In our case, however, the mass for the motion parallel to the dimer direction is inverted. Thus the dimer accelerates opposite to the direction of the force. Thus a friction acting on the dimer via the electrons leads to a velocity-dependent acceleration of the dimer, which may cause an instability of the dimer motion.

The detrimental effect of the wave function motion can be avoided by choosing a sufficiently small mass for the wave function dynamics or by artificially increasing the atomic masses. In our study, we used a mass of 50 u for all atoms. The wave functions have been kept close to the ground state by applying a friction that dissipates 2% of the kinetic energy in each time step.

The dimensionless masses for the dimer motion have been chosen to be

$$M_{\parallel} = -1.00, \tag{55}$$

$$M_{\perp} = +1.00, \tag{56}$$

$$M_{\circ} = +0.25. \tag{57}$$

The small value for $M_{\circ}$ has been chosen to speed up the reorientation of the dimer.

In order to avoid instabilities, we found it useful to introduce an upper limit to the kinetic energy individually for the rotational, perpendicular, and parallel motions. These limits were enforced by adjusting the frictions accordingly. The limit for the kinetic energy $E_{\mathrm{kin,max}}$ is translated into an upper "temperature" T_{max} according to

$$\tfrac{1}{2} g k_B T_{\mathrm{max}} = E_{\mathrm{kin,max}}, \tag{58}$$

where g is the number of degrees of freedom in the corresponding motion type and k_B is Boltzmann's constant.

Within the limits of the enforced maximum kinetic energies, we adapted the friction dynamically in each step to come close to the limit of critical damping. The latter results in the best possible convergence behavior.

Furthermore, the friction is increased to a higher value specified by the user, if the dimer moves away from the stable point. The decision to increase the friction has been made on the basis of the actual forces and velocities. In our simulation we have chosen this friction so that the energy dissipated per time step corresponds to 20% of the kinetic energy of the corresponding type of motion.

When starting the dimer simulation, it is important to optimize the dimer orientation, i.e., $\mathbf{Y}_1$, first, before the mean dimer configuration $\mathbf{Y}_2$ changes appreciably. This is because the mean dimer configuration only approaches the transition state if the dimer orientation is sufficiently aligned along the unstable vibrational mode of the transition state.

The dimer orientation can be optimized in different ways. (1) Starting from initial dimer coordinates, the mean dimer configuration $\mathbf{Y}_1$ is constrained to the initial value, while the orientation $\mathbf{Y}_2$ is fully optimized. Only after this optimization also the mean configuration is allowed to move. (2) Starting from one monomer configuration, the second monomer is constructed from the first by letting it follow the forces until the desired dimer length is obtained. We will refer to this technique as the "growing dimer technique." (3) Starting from a dimer with the monomers being identical to the two metastable minima, the dimer length is successively shortened, while the dimer position is optimized. Results for all three optimization strategies can be found in Table I.

We found that the third strategy suffers from the fact that additional effort is required to contract the dimer length to the desired value. It also suffers from an instability caused by strong anharmonic effects.

The growing-dimer technique has the advantage that the second monomer is constructed dynamically from the first, without the need of an independent optimization of the wave functions. In the growing dimer technique the dimer orientation is optimized automatically as soon as the targeted dimer length is reached. In the first strategy the orientation is obtained during the first iterations with a constrained mean dimer configuration.

We will discuss here the first strategy. The initial structure of the dimer is given by a mean dimer configuration midway between the two metastable states (A) and (B). The dimer length is chosen such that the distance of the two monomers in coordinate space is 0.33 Å.

During the first 700 time steps, the dimer orientation has been optimized. Here the mean dimer configuration has not been constrained, but the maximum temperature for the perpendicular motion has been kept at a small value of 10 K. For the parallel and rotational motions, the maximum tem-

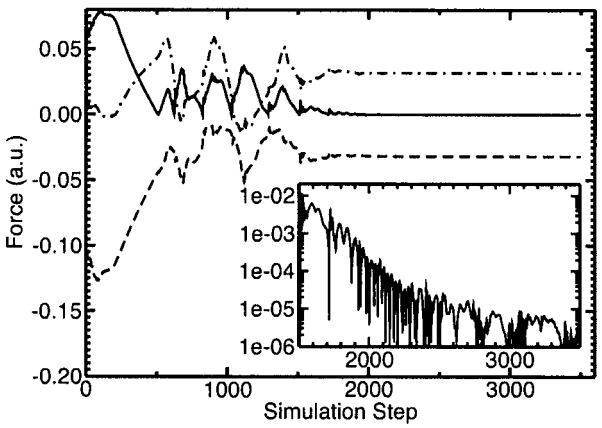

FIG. 5. Forces over time step for a calculation following optimization strategy (1) described in the text. The dashed and dash-dotted lines show the forces parallel to the dimer axis for images one and two, respectively. The full line corresponds to the resulting force acting on the center of gravity of the dimer. The logarithmic scale of the inset provides detailed information for the latter.

perature has been set to 500 K. After the first 700 time steps the maximum temperature for the perpendicular motion has been increased to 500 K. In Figs. 5 and 6 we show the convergence of the forces for the parallel, rotational, and perpendicular motions. Good convergence is reached after 2000 time steps. The estimates for the transition state energy and the deviation of the mean dimer configuration from the transition state is given in Table I.

VI. SUMMARY

A formulation of the dimer method for searching transition states is presented which can be used in *ab initio* molecular dynamics simulations using a fictitious Lagrangian. The dimer method is successful in cases where the widely used drag method fails. We investigate the dynamics close to the stable points of the dimer analytically. In addition we demonstrate the performance of our implementation using a practical example typically used as test case for transition state search algorithms, namely, the conrotatory ring opening of (chloro-) cyclobutene.

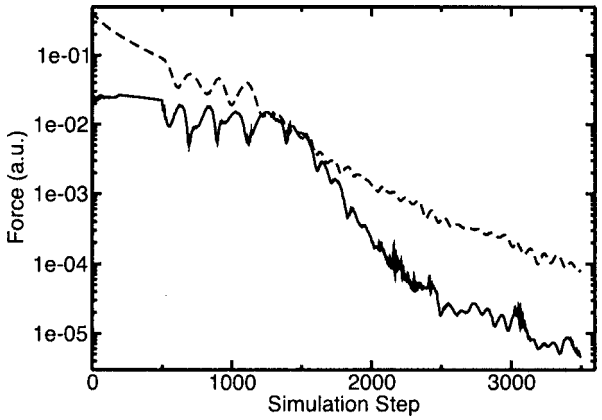

FIG. 6. Rotational (full line) and perpendicular (dashed line) parts of the forces acting on the dimer over time steps for a calculation following optimization strategy (1) described in the text.

APPENDIX A: COMPUTATIONAL DETAILS

We performed density functional calculations[28,29] based on the projector augmented wave (PAW) method.[30,31] The gradient-corrected PBE (Ref. 32) functional was used for exchange and correlation. The PAW method is a frozen-core all-electron method. Like other plane wave based methods, the PAW method leads to the occurrence of artificial periodic images of the structures. This effect was avoided by explicit subtraction of the electrostatic interaction between them.[33] Wave function overlap was avoided by choosing the unit cell large enough to keep a distance of more than 6 Å between atoms belonging to different periodic images. We used a plane wave cutoff of 30 Ry for the auxiliary wave functions of the PAW method. The following sets of projector functions were employed: Cl $2s2p1d$, C $2s2p1d$, and H $2s1p$. These provide the number of projector functions per angular momentum magnetic quantum number m in each main angular momentum channel ℓ.

Atomic structures were optimized by damped Car-Parrinello[34] molecular dynamics. We used a time step of 10 a.u. (2.5 fs) for all except the dynamical dimer calculations. See Sec. V B for further details. The convergence was tested by monitoring if the total energy change remains below 10^{-5} hartree during a simulation of 500 time steps. During the simulation for the convergence test, no friction was applied to the atomic motion, and the friction on the wave function dynamics was chosen sufficiently low to avoid a noticeable effect on the atomic motion.

[1] H. Eyring, J. Chem. Phys. **3**, 107 (1934).
[2] G. Vineyard, J. Phys. Chem. Solids **3**, 121 (1957).
[3] J. Keck, Discuss. Faraday Soc. **33**, 1962 (1962).
[4] D. Poppinger, Chem. Phys. Lett. **35**, 550 (1975).
[5] C. J. Cerjan and W. H. Miller, J. Chem. Phys. **75**, 2800 (1981).
[6] J. Baker, J. Comput. Chem. **7**, 385 (1986).
[7] J. Simons, P. Jorgensen, H. Taylor, and J. Ozment, J. Phys. Chem. **87**, 2745 (1983).
[8] A. Banerjee, N. Adams, J. Simons, and R. Shepard, J. Phys. Chem. **89**, 52 (1985).
[9] L. J. Munro and D. J. Wales, Phys. Rev. B **59**, 3969 (1999).
[10] H. Jonsson, G. Mills, and K. W. Jacobsen, *Classical and Quantum Dynamics in Condensed Phase Simulations*, edited by B. J. Berne, G. Ciccotti, and D. F. Coker (World Scientific, Singapore, 1998), p. 385.
[11] G. Mills and H. Jonsson, Phys. Rev. Lett. **72**, 1124 (1994).
[12] G. Mills, H. Jonsson, and G. Schenter, Surf. Sci. **324**, 305 (1995).
[13] R. Malek and N. Mousseau, Phys. Rev. E **62**, 7723 (2000).
[14] W. E. W. Ren and E. Vanden-Eijnden, Phys. Rev. B **66**, 052301 (2002).
[15] B. Peters, A. Heyden, A. T. Bell, and A. Chakraborty, J. Chem. Phys. **120**, 7877 (2004).
[16] G. Henkelman, G. Johannesson, and H. Jonsson, *Progress on Theoretical Chemistry and Physics*, edited by S. D. Schwartz (Kluwer Academic, Dordrecht, 2000), p. 269.
[17] H. B. Schlegel, J. Comput. Chem. **24**, 1514 (2003).
[18] G. Henkelman and H. Jonsson, J. Chem. Phys. **111**, 7010 (1999).
[19] R. A. Olsen, G. H. Kroes, G. Henkelman, A. Arnoldsson, and H. Jonsson, J. Chem. Phys. **121**, 9776 (2004).
[20] R. Car and M. Parrinello, Phys. Rev. Lett. **55**, 2471 (1985).
[21] Y. Kanai, A. Tilocca, A. Selloni, and R. Car, J. Chem. Phys. **121**, 3359 (2004).
[22] J.-P. Ryckaert, G. Ciccotti, and H. J. C. Berendsen, J. Comput. Phys. **23**, 327 (1977).
[23] R. B. Woodward and R. Hoffmann, J. Am. Chem. Soc. **87**, 395 (1965).
[24] M. J. S. Dewar and S. Kirschner, J. Am. Chem. Soc. **93**, 4292 (1971).

[25] J. Breulet and H. F. Schaefer, J. Am. Chem. Soc. **106**, 1221 (1984).
[26] J. M. Olivia, J. Gerratt, P. B. Karadakov, and D. L. Cooper, J. Chem. Phys. **107**, 8917 (1997).
[27] See EPAPS Document No. E-JCPSA6-128-004803 for the coordinates of the structures disussed. This document can be reached through a direct link in the online article's HTML reference section or via the EPAPS homepage (http://www.aip.org/pubservs/epaps.html).
[28] P. Hohenberg and W. Kohn, Phys. Rev. **136**, B864 (1964).
[29] W. Kohn and L. Sham, Phys. Rev. **140**, A1133 (1965).
[30] P. E. Blöchl, Phys. Rev. B **50**, 17953 (1994).
[31] P. E. Blöchl, C. Först, and J. Schimpl, Bull. Mater. Sci. **26**, 33 (2003).
[32] J. Perdew, K. Burke, and M. Ernzerhof, Phys. Rev. Lett. **77**, 3865 (1996).
[33] P. E. Blöchl, J. Chem. Phys. **103**, 7422 (1986).
[34] R. Car and M. Parrinello, Phys. Rev. Lett. **55**, 2471 (1985).